Environmental Technology & Innovation 23 (2021) 101625

Contents lists available at ScienceDirect

Environmental Technology & Innovation

journal homepage: www.elsevier.com/locate/eti

Optimal degradation of Ciprofloxacin in a heterogeneous Fenton-like process using (δ-FeOOH)/MWCNTs nanocomposite

Marjan Salari [a], Gholam Reza Rakhshandehroo [b], Mohammad Reza Nikoo [b,*], Mohammad Mahdi Zerafat [c], Mehrdad Ghorbani Mooselu [d]

[a] Department of Civil and Environmental Engineering, Sirjan University of Technology, Kerman, Iran
[b] Department of Civil and Environmental Engineering, Shiraz University, Shiraz, Iran
[c] Faculty of Advanced Technologies, Nanochemical Engineering Department, Shiraz University, Shiraz, Iran
[d] Department of Engineering and Science, University of Agder, Norway

ARTICLE INFO

Article history:
Received 6 November 2020
Received in revised form 22 April 2021
Accepted 12 May 2021
Available online 19 May 2021

Keywords:
Ciprofloxacin antibiotic
(δ-FeOOH)/MWCNTs nanocomposite
Central composite design (CCD)
Feroxyhyte
Heterogeneous Fenton-like process

ABSTRACT

This study was aimed at the synthesis and characterization of (δ-FeOOH)/MWCNTs nanocomposite as the catalyst for Ciprofloxacin (CIP) removal through a heterogeneous Fenton-like process. The proposed experimental design applies the central composite design (CCD) as a response surface methodology (RSM). The effect of influential parameters, including initial CIP concentration, catalyst dose, H_2O_2 concentration, initial pH, and reaction time on removal, were investigated. (δ-FeOOH)/MWCNTs nanocomposite was synthesized using a single-step co-precipitation technique. Besides, nanoferoxyhyte and nanocomposite properties were characterized by transmission electron microscopy(TEM), Fourier-transform infrared spectroscopy (FTIR), energy dispersive X-ray analysis (EDX), particle size analysis (PSA), X-ray diffraction (XRD), vibrating sample magnetometer (VSM) and field emission scanning electron microscopy (FESEM). The inhibitory hale experiment was performed by Escherichia coli (E. coli) to evaluate the antibacterial activity. The optimal CIP removal efficiency (86.9%) was achieved by 131.6 min reaction time, CIP concentration of 10.0 mg/L, catalyst dosage of 23.5 mg, H_2O_2 concentration of 20.6 mM, and initial pH of 5.3, with a biodegradability index (BOD_5/COD) of 0.35 Based on the results, (δ-FeOOH)/MWCNTs showed a significant catalytic activity for CIP removal, which can be attributed to the simultaneous effects of advanced oxidation and absorption.

1. Introduction

Pharmaceuticals are classified as priority risk pollutants considered a widespread environmental issue (Hernando et al., 2006; Watkinson et al., 2007; De Lima Perini et al., 2014). Among these, antibiotics may cause antimicrobial resistance among microorganisms in wastewaters and increase the bacterial resistance (Levy, 1998; Kümmerer, 2004, 2009; Haddad and Kümmerer, 2014). Ciprofloxacin (CIP) belongs to the second generation of Fluoroquinolones (FQs) broadly implemented for the treatment of humans and animals (De Lima Perini et al., 2014). Improper consumption of

* Corresponding author.
E-mail addresses: m.salari@sirjantech.ac.ir (M. Salari), rakhshan@shirazu.ac.ir (G.R. Rakhshandehroo), nikoo@shirazu.ac.ir (M.R. Nikoo), mmzerafat@shirazu.ac.ir (M.M. Zerafat), Mehrdad.g.mooselu@uia.no (M.G. Mooselu).

https://doi.org/10.1016/j.eti.2021.101625
2352-1864/

these drugs can pose serious threats to the ecosystem and human health (Golovko et al., 2014; Lima et al., 2017). Due to high solubility in aqueous media and high stability in soil and sewage environments, CIP removal from water sources is an essential task in wastewater treatment (Zhuang et al., 2015; Rakhshandehroo et al., 2018; Salari et al., 2018a,b, 2019).

Among different water treatment techniques, advanced oxidation based on Fenton's chemistry is proved very successful for degradation of various contaminants (Chen et al., 2015; Asghar et al., 2014; Giri and Golder, 2015; Gupta and Garg, 2018). Homogeneous Fenton process is performed via activating OH° radicals as highly oxidative agents as an economical and environmentally friendly treatment technique. However, the typical homogeneous Fenton process operates only within a strictly optimal pH range (usually pH < 3.5) and produces a huge amount of lead sludge that increases the treatment cost. To solve these limitations, a heterogeneous Fenton process is used in the solid phase utilizing a porous substrate (Shukla et al., 2010; Maa et al., 2015), to prevent iron sludge production and extend the effective pH range. Besides, reuse capability increases the process benefits (Garrido-Ramírez et al., 2010).

Therefore, a broad range of materials such as zeolites (Kasiri et al., 2008), activated carbon (Shahidi et al., 2018), oxide minerals (Yeh et al., 2008), graphene oxide (Yao et al., 2014), and clays (Iurascu et al., 2009) have been used as the solid substrate. Recently, heterogeneous Fenton-like catalysts are produced with a high specific surface area and used to effectively degrade the organic pollutants (Nie et al., 2015; Chen et al., 2009). Carbon nanotubes (CNTs), with unique characteristics and great advantages such as being inexpensive, non-toxic, and fairly stable while having a huge specific surface area (Zhang et al., 2010; Cui et al., 2013) are widely utilized as the Fenton catalytic support. CNTs have excellent mechanical (Chen et al., 2003), electrical conductivity (Xu et al., 1999), magnetic (Zhan et al., 2003), corrosion resistance (Dhinakaran et al., 2013; Chen et al., 2005), and unique electronic and thermal stability properties (Kuzumaki et al., 1998; Andrews et al., 1999) which make them a great alternative as the support material in heterogeneous Fenton catalysis. Also, the large surface area and stability suggest CNTs as the ideal material for hosting other nanoparticles (Kaur et al., 2015). CNTs could be decorated with nanoparticles due to their extensive potential for adsorption and catalysis (Gul et al., 2010; Wan et al., 2015). In particular, multi-walled Carbon nanotubes (MWCNTs) have been used as the carrier for nanoparticles to increase the catalytic activity via heterogeneous reactions (e.g., Fenton in organic pollutants' degradation). Among heterogeneous Fenton-like catalysts, iron nanoparticles such as magnetite (Fe_3O_4), goethite (α-FeOOH), and pyrite (FeS_2) are broadly used due to relatively extensive affinity for soils and simple operating conditions (Cui et al., 2013).

The novelty of this study lies in determining the synthesis and characterization of (δ-FeOOH)/MWCNTs nanocomposite and optimization of heterogeneous Fenton-like process for removal of CIP antibiotic using central composite design (CCD) under response surface methodology (RSM). At optimal conditions, the biodegradability index (BOD_5/COD) of the CIP solution before and after the removal process was calculated. Also, the inhibitory hale experiment was performed by Escherichia coli (E. coli) to evaluate the antibacterial activity. A simple synthetic route was proposed to prepare (δ-FeOOH)/MWCNTs nanocomposite through the co-precipitation technique.

Moreover, properties of this nanocomposite were investigated using various characterization techniques such as particle size analysis (PSA), field emission scanning electron microscopy (FESEM), Fourier-transform infrared spectroscopy (FTIR), transmission electron microscopy (TEM), X-ray diffraction (XRD), vibrating sample magnetometer (VSM) and energy dispersive X-ray analysis (EDX). Based on the literature, the as-prepared nanocomposite has never been used as a Fenton-like catalyst previously.

2. Materials and methods

The proposed methodology for synthesis and optimization of (δ-FeOOH)/MWCNTs nanocomposite for CIP removal consists of 3 main steps (Fig. 1), including the synthesis and characterization of feroxyhyte (δ-FeOOH) nanoparticles (step1), optimization of heterogeneous Fenton-like experiments using RSM (step 2), and optimization of parameters to synthesize feroxyhyte (δ-FeOOH) nanoparticles (step 3). A simple synthetic route was proposed to prepare (δ-FeOOH)/MWCNTs nanocomposite through the co-precipitation technique. Each main section was divided into sub-sections according to Fig. 1.

The applied reagents in this research, including CIP ($C_{17}H_{18}FN_3O_3$, 98%) and MWCNTs (> 95%), ferrous chloride ($FeCl_2.4H_2O$, 99.5%), sulfuric acid (H_2SO_4, 95%–97%), sodium hydroxide (NaOH, 97%), potassium hydroxide (KOH, 85%), Ethylene glycol (EG, 99.5%), Nitric Acid (HNO_3, 70%) and hydrogen peroxide (H_2O_2, 30%) were supplied by Merck Co. (Germany) and used as received without further purification.

2.1. Synthesis and characterization of (δ -FeOOH)/MWCNTs nanocomposite

2.1.1. MWCNTs functionalization

First, MWCNTs were functionalized via the reflux technique to activate the attachment of the metal on the surface. Accordingly, 2 g of MWCNTs were dispersed in 110 ml of HNO_3, and 75 ml of deionized water was added to the acidic solution to achieve the desired molarity. The mixture was refluxed at 200 °C under magnetic stirring for 6 h. Then, MWCNTs were washed with deionized water several times to remove residues and reduce the pH values below 7. The purified samples were collected by centrifugation at 4000 rpm, and the samples were dried in the oven (Aboutalebi et al., 2011; Kaur et al., 2015).

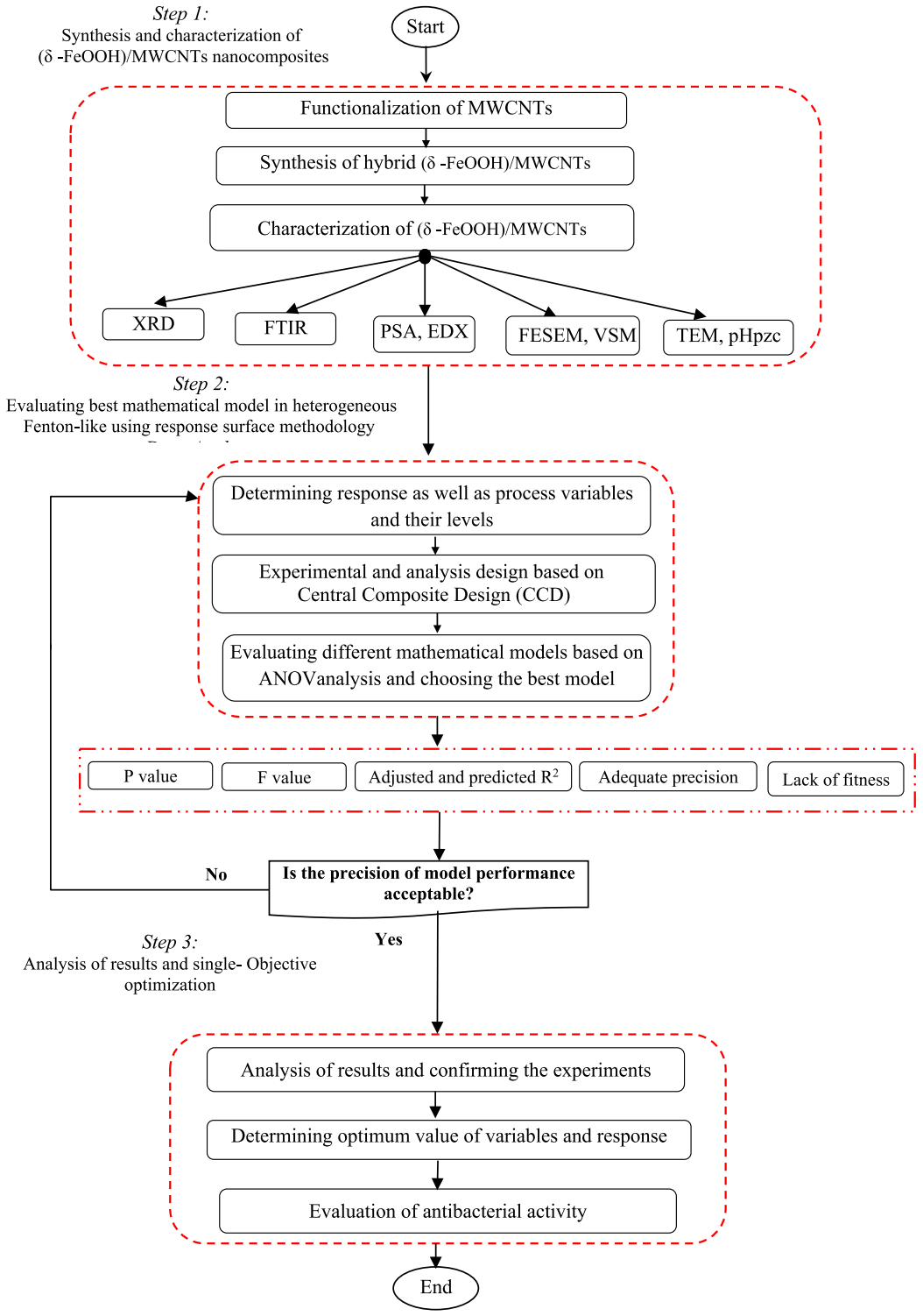

Fig. 1. The proposed method for CIP removal using feroxyhyte (δ-FeOOH)/MWCNTs nanocomposite.

2.1.2. Synthesis of (δ-FeOOH)/MWCNTs nanocomposite

Preparation of (δ-FeOOH)/MWCNTs nanocomposite was performed using the co-precipitation technique (Carlson and Schwertmann, 1980). The agglomeration tendency of pristine MWCNTs in various solvents leads to non-uniform

dispersion. To solve this problem, the functionalization of MWCNTs using nitric acid has been widely reported (Carlson and Schwertmann, 1980). In this study, MWCNTs were functionalized using nitric acid at the first step, and δ-FeOOH nanoparticles were attached to MWCNTs at the next step. Then, 0.2 g of the functionalized MWCNTs and 0.5 g of $FeCl_2.4H_2O$ were added to 200 mL of deionized water, and the suspension was ultrasonicated for 20 min. Meanwhile, 7 mL of ethylene glycol (EG) was added to the suspension. Upon complete dissolution of $FeCl_2.4H_2O$, the suspension was transferred to an oil bath and heated up to 95 °C under severe mechanical stirring. Then, 5 M of KOH was added dropwise under constant stirring to obtain pH of 8, where oxidation is completed within a few seconds after the addition of excess H_2O_2. In the next step, 15 mL of H_2O_2(30%) was added quickly, and flocculation was improved by dropwise addition of 5 M KOH to obtain pH of 8. pH not only affects the adsorbent surface properties but also determines various ionic forms of CIP (Peng et al., 2015). The prepared suspension was maintained at 95 °C for 2 h and cooled down to room temperature. Finally, the precipitate was dried at 45 °C in vacuum oven for 18 h, and (δ-FeOOH)/MWCNTs nanocomposite was analyzed using various characterization techniques.

2.1.3. Characterization of δ-FeOOH nanoparticles and (δ-FeOOH)/MWCNTs nanocomposite

X-ray diffraction (XRD) pattern of functionalized MWCNTs, feroxyhite nanoparticles, and feroxyhite/MWCNT nanocomposite was prepared to determine the crystalline phases, and experiments were conducted to investigate the structural phases using an XPertpro X-ray diffractometer (Cu Ka radiation, k = 1.5406) over the 2θ=20–80^0 range at 30 mA and 40 kV, with a scanning rate of 1/min and 0.02 step size. Crystallite size (ξ) was determined using Scherer formula and full width at half maximum (FWHM) method (Eq. (1)), from the width of the most intensive XRD peak at 2θ=35° (Alexander and Klug, 1950):

$$\xi = \frac{k\lambda}{\beta \cos\theta} \tag{1}$$

The X-ray spectrum consists of a continuous distribution, on which the characteristic line spectrum of copper (k) was superimposed ($k = 0.94$). In Eq. (1), X-ray wavelength (λ) is mainly 0.154 nm, Crystallite size (β) = 0.00549 A, and the width of the most intensive XRD peak occurs at 2θ = 35 °C.

FTIR was performed using a Nicolet Nexus infrared spectrometer to determine the functional groups in the prepared samples. Also, Field Emission Scanning Electron Microscopy (FE-SEM) was implemented to observe the morphology and size of the nanocomposite. The morphology and size of the as-prepared sample were investigated by transmission electron microscopy (TEM). Also, each peak appearing on the EDX graph is related to a particular atom, where higher altitudes show higher concentrations of the element in the sample (Khodadadi et al., 2017). TEM observation with a line resolution of 3 A° and an operating voltage of 120 kV was carried out using a TEM LEO 912 AB.2.3 device. Magnetic properties of the synthesized nanoparticles were investigated using a Vibrating Sample Magnetometer (VSM). The point of zero charge (PZC) of MWCNT and the nanocomposite were determined according to previous studies (Fayazi et al., 2015).

2.2. Optimization of heterogeneous Fenton-like experiments using RSM

2.2.1. Analytical procedure

Batch experiments were conducted to evaluate CIP removal by the nanocomposite. For this purpose, 500 mg of CIP was dissolved in 1 L of distilled water to obtain the stock solution with a concentration of 500 mg/L. The stock solution was diluted using distilled water to obtain the required concentrations. During the experiment, sampling was performed according to the CCD design. Solution pH was adjusted using NaOH and H_2SO_4 (1 M). A defined amount of nanocomposite was then put in a 100 ml solution with the required CIP concentration. Heterogeneous Fenton-like experiments were performed under a shaker upon addition of hydrogen peroxide (H_2O_2, 30% (w/w)).

Next, nanoparticles were sedimented in the specimens, and the specimens were filtered using a syringe equipped with a 0.45 μm filter. Then, CIP concentration was determined using UV–Vis spectrophotometer (DR 5000) at a 277 nm wavelength. Also, the concentration of residual CIP at optimal conditions was determined using high-performance liquid chromatography equipped with a UV lamp detector (HPLC-UV). The mobile phase contained a mixture of acetic acid and acetonitrile with a 80:20 volume ratio. An injection flow rate of 1.0 mL.min^{-1} and a total injection volume of 15 μL were utilized. CIP degradation ratio (Dr) was calculated by Eq. (2):

$$Dr(\%) = \left(\frac{C_0 - C_f}{C_0}\right) \times 100 \tag{2}$$

Where, C_0 and C_f are initial and final CIP concentrations (mg/L), respectively. The nanocomposite from outlet solutions was separated by centrifugation for 8 min at 3900 rpm and then filtration with the 0.22 μm polytetra fluoroethylene syringe filter.

2.3. Optimization of heterogeneous Fenton-like experiments using RSM

Response surface methodology (RSM) includes a group of mathematical and statistical techniques for the design of experiments. For this purpose, Design-Expert software (DX10) was implemented as a reliable tool. It is used for modeling and analyzing where a process response is influenced by several input variables, as well as optimization of this specific response (Amiri and Sabour, 2014). RSM with CCD is designed by fitting an empirical model to the experimental data (APHP, 2005; Zubir et al., 2015; Khataee et al., 2012).

In this study, experimental results were analyzed using a response surface regression procedure in experimental design and also by applying statistical analysis. Usually, a first- or second-order model was used to find an appropriate approximation for the functional relationship between the independent variables and the objective function based on Eq. (3) (APHP, 2005; Khataee et al., 2012):

$$Y = \beta_0 + \sum_{i=1}^{k} \beta_i X_i + \sum_{i=1}^{k} \beta_{ii} X_{ii}^2 + \sum_{i<j} \beta_{ij} X_i X_j + e(X_1.X_2, \ldots, X_k) \quad (3)$$

Where, Y is the predicted response, X_i and X_j are coded variables for independent variables, β_0 is an intercept, β_i is the linear coefficient, β_{ii} shows the quadratic coefficient, and β_{ij} indicates the interaction coefficient (APHP, 2005; Khataee et al., 2012).

In this work, five factors were selected as independent variables, including initial CIP concentration (*A*, mg/L), catalyst dose (*B*, mg), H_2O_2 concentration (*C*, mM), initial pH (D) and the reaction time (E, min). Forty-five experiments were designed with five variables, each with five levels (Table S1). Among these 45 experiments, three experiments were repeated at the central point (runs # 11, 39, and 44). Matching responses for these three experiments were considered as a sign of accuracy for the experimental procedure (Azami et al., 2012).

CIP removal was selected as the response variable (see Table S1 in Electronic Supplementary Material (ESM)). Operational ranges for experimental parameters were determined based on the results of preliminary experiments and previous reports (Lak et al., 2012; Maa et al., 2015). CCD has the maximum efficiency for an RSM problem involving five variables and five levels. The proposed CCD requires 45 runs to model a response surface. Furthermore, analysis of variance (ANOVA) was utilized for statistical analysis of the experiments.

2.4. Antibacterial activity

The inhibitory hale experiment was performed to evaluate the antibacterial activity. In various studies, Escherichia coli (E. coli) has been used as an indicator for the estimation of antibacterial activity residues (Gupta and Garg, 2018; Ye et al., 2016; DeBel et al., 2009). On the other hand, E. coli bacterium from the Enterobacteriaceae family is the most common cause of urinary tract infections. In this study, E. coli was cultured in sterile conditions, firstly using a calibrated loop (0.1 ml) on Blood Agar (BA) and Eosin Methylene Blue Agar (EMBA). Afterward, 10 μl of the untreated and refined antibiotics were dispersed at different times in the plates containing the bacterial culture. The plates were then cultured in an incubator at 37 °C for 24 h. Finally, the antibacterial activity of the CIP antibiotic was evaluated qualitatively through inhibitory hale.

3. Results and discussion

3.1. Characterization of (δ-FeOOH)/MWCNTs nanocomposite

Characterization of (δ-FeOOH)/MWCNTs nanocomposite is presented in Fig. S1, in which Fig. S1.a illustrates the XRD patterns, and Fig. S1b shows the FTIR spectra for pure MWCNTs, HNO_3-treated MWCNTs, feroxyhyte nanoparticles, and the nanocomposite. For MWCNTs functionalized with nitric acid, the characteristic CNT peaks at 26.46° and 44.97°, are ascribed to (011) and (021) crystalline planes, respectively. This shows that the MWCNTs structure was not destroyed upon acid treatment (Kuzumaki et al., 1998). For the hexagonal feroxyhyte crystalline structure (JCPDS 65-3107), six peaks were found at 2θ values, including 35°, 39°, 40°, 53°, 63°, and 72°, corresponding to (010), (002), (011), (012), (110), and (103) crystalline planes, respectively. As calculated by Scherer's formula (Eq. (1)), the average crystallite sizes were ∼22 and 31 nm for feroxyhyte nanoparticles and the nanocomposite, respectively. Upon attachment of feroxyhyte onto MWCNTs, six XRD peaks of the feroxyhyte phase remained unchanged, and no other peak corresponding to impurities was detected. It should be noted that the minimum dose of the required nanocomposite as the initiator/agent of degradation is among the main parameters in the process design.

FTIR is used for investigating the functional groups on the surface of adsorbent particles (Khataee et al., 2012). It was used to investigate the chemical bonds and functional groups on the surface of CNTs functionalized using nitric acid. FTIR spectra shows the interactions during adsorption onto the nanotubes, nanoparticles, and nanocomposite (Khataee et al., 2012). Fig. S2b indicates the unchanged structure of MWCNTs upon functionalization by nitric acid. The wavenumber 3447 cm^{-1} was attributed to either OH bond in carboxylic groups or water adsorption. Lower wavenumbers indicate stronger hydrogen bonds between -OH groups (DeBel et al., 2009; Lak et al., 2012; Ye et al., 2016; Kakavandi et al., 2016).

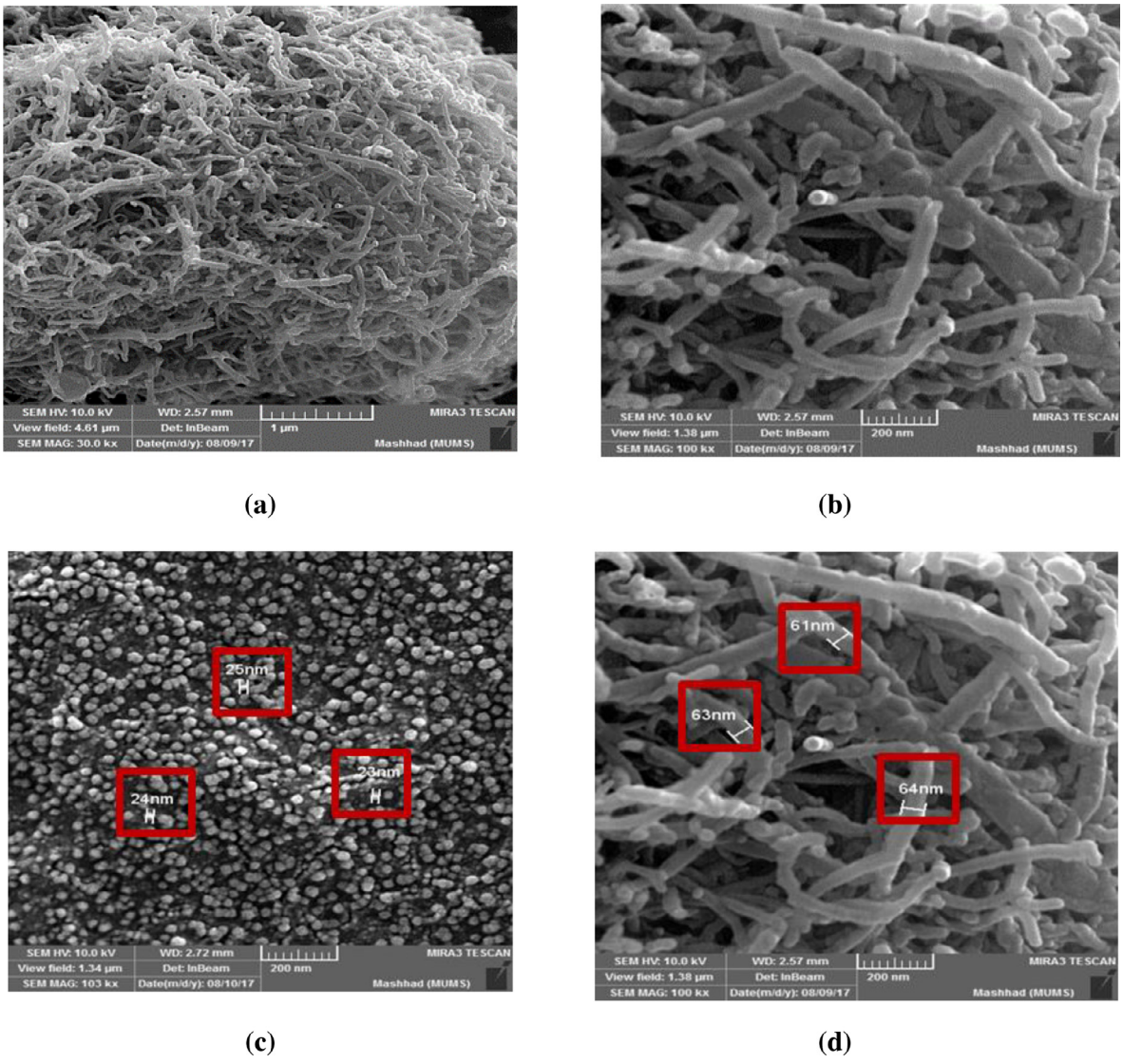

Fig. 2. FESEM images for (a) pure MWCNTs, (b) acid-treated MWCNTs, (c) (δ-FeOOH) Nanoparticles and (d) (δ-FeOOH)/MWCNTs Nanocomposite.

Peaks in the 2846–2856 cm $^{-1}$ range, may be attributed to the symmetric and asymmetric -CH tensile vibration modes (Lak et al., 2012). The absorption peak at wavenumber 1169–1629 cm $^{-1}$ was attributed to MWCNTs bound to the carboxylic group (-COOH) bonded to the carbonyl group of the quinine, or the ring structure. Apparently, the formation of such functional groups during MWCNTs synthesis would provide conditions for easier bonding of feroxyhyte onto MWCNTs through the hydrogen bond. Absorption peaks for MWCNTs functionalized by nitric acid at 1690 cm^{-1} and 1629 cm $^{-1}$ wavenumbers were attributed to the carboxylic group (-COOH) bonded to the carbonyl group of the quinine, or the ring structure (Gul et al., 2010). However, such peaks are weakened, or in some areas disappeared, in the (δ-FeOOH)/MWCNTs spectrum. Apparently, such functional groups are disappeared during synthesis. Wavenumbers in the 1000–1350 cm^{-1} range were attributed to C–F stretching bonds under various chemical environments (Khodadadi et al., 2017). Finally, the infrared spectrum shows Fe–O bonds at wavenumbers lower than 700 cm $^{-1}$. Peaks at 1628.25, 1383.51, and 1174.46 cm^{-1} were attributed to C=O, n (CH_2), and C–O functional groups, respectively. It was concluded that the presence of feroxyhyte and MWCNTs in the composite specimen was approved.

Fig. 2 displays the FESEM images for pure MWCNTs, MWCNTs+HNO_3, feroxyhyte, and (δ-FeOOH)/MWCNTs nanocomposite. As shown, MWCNTs diameter and length were 20–30 nm and 10-20 μm, respectively.

TEM images for feroxyhyte nanoparticles and (δ-FeOOH)/MWCNTs nanocomposite are given in Fig. 3. For TEM test, samples were prepared under ultrasonication in ethanol for a certain period. Fig. 3a reveals that feroxyhyte nanoparticles have a hexagonal structure, a similar conclusion to that of other reports (e.g., Carlson and Schwertmann, 1980; Sestu

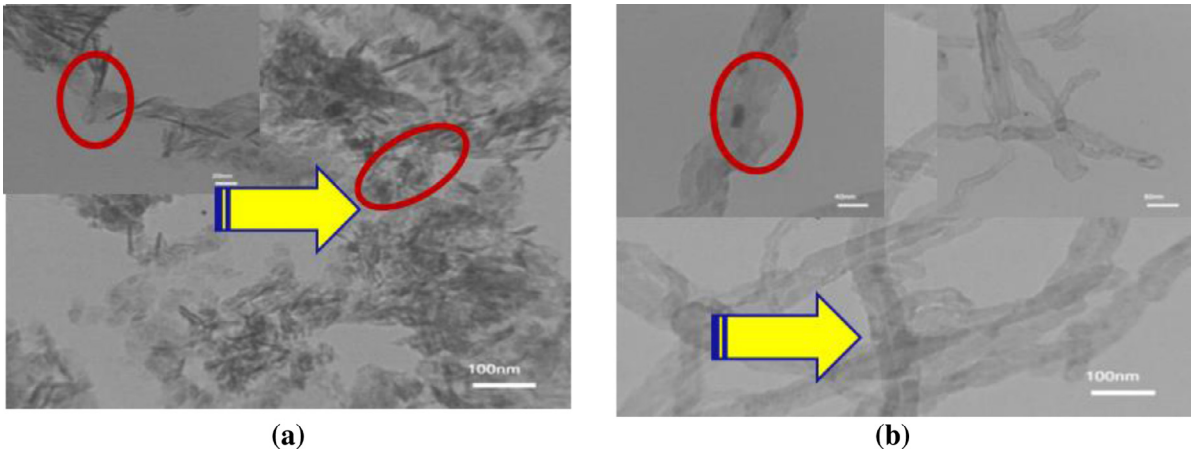

Fig. 3. TEM images for (a) feroxyhyte nanoparticles and (b) (δ-FeOOH)/MWCNTs nanocomposite.

et al., 2015). Fig. 3b illustrates that feroxyhyte nanoparticles were attached to the surface of functionalized MWCNTs. It was concluded that almost all nanoparticles were placed on the surface of functionalized MWCNTs, suggesting a bond between nanoparticles and MWCNTs.

Particle size analysis (PSA) for feroxyhyte nanoparticles and the fitted Gaussians equation are presented in Fig. S2. Based on Fig. S2, the average diameter of the nanoparticles was 17.17 nm.

Magnetic properties of pure feroxyhyte nanoparticle (δ-FeOOH) and (δ-FeOOH)/MWCNTs nanocomposite were measured using VSM in a $\pm$10 kOe field at room temperature (Fig. S3). Based on the results, both samples were paramagnetic at room temperature with no hysteresis. The saturation magnetization (Ms) for the nanocomposite was 42 emu/g; significantly less than that of the feroxyhyte nanoparticle (60 emu/g). However, (δ-FeOOH)/MWCNTs were paramagnetic with a lower saturation magnetization. The reduction in the saturation of nanocomposite was ascribed to size effect, lower iron content in the nanocomposite, and the presence of non-magnetic materials. The lower saturation magnetization and low coercivity indicate that (δ-FeOOH)/MWCNTs might be separated from the treated solution easily by implementing an external magnetic field.

Chemical purity of samples and stoichiometry of pristine MWCNTs, functionalized MWCNTs, feroxyhyte nanoparticles, and nanocomposite were examined by EDX analysis. The elemental analysis from the highlighted area is shown in Fig. 4 (inset). The standard EDX range recorded on the samples is also shown in Fig. 4. The spectrum for feroxyhyte nanoparticles and nanocomposite clearly shows five peaks between 0.2 and 9 keV (Fig. 4). As shown in Fig. 4c, most peaks are related to iron and carbon elements with characteristic lines L and K. Also, in Fig. 4d, the maximum peak at 0.2 keV located on the left is related to carbon. The oxygen characteristic line, which is hardly visible, is located at 0.3 keV. Carbon and oxygen points in samples confirm the presence of stabilizers consisting of alkyl chains. Chemical analysis performed by EDX revealed that the nanocomposite contains ~51.38% carbon, 30.43% oxygen, and 18.19% iron. Finding strong peaks corresponding to C and Fe in the spectrum reflects the presence of carbon and iron in the nanocomposite structure.

After producing the nanocomposite, the surface charge is determined by pH_{pzc} measurement test. Based on Fig. S4, pH_{pzc} of MWCNTs, and (δ-FeOOH)/MWCNTs nanocomposites were 3.92 and 4.36, respectively.

3.2. Effects of various parameters on CIP degradation

Results obtained by the CCD experimental design for degradation of CIP by (δ-FeOOH)/MWCNTs in a Fenton-like process are presented in Table 1. In order to predict the optimal values for CIP removal at the laboratory conditions, a second-order polynomial was fitted to the experimental data. Eq. (4) is a quadratic polynomial showing the relation between CIP removal rate and independent input variables:

$$Y = +60.54 - 2.43A + 1.00B + 1.18C + 2.58D - 3.41E + 4.63A^2 + 1.44C^2 - 4.19D^2 + 2.31E^2 \quad (4)$$

In Eq (4), the positive (negative) sign for this purpose is that the variable is directly (inverse) proportional to the response. It should be noted that only significant terms (with a P-value < 0.05 for Y) were selected to be included in the reduced quadratic equation, where A, B, C, D, E and Y are CIP concentration (mg/L), the dose of (δ-FeOOH)/MWCNTs (mg), H_2O_2 concentration (mM), initial pH, time and CIP removal (%), respectively. The performance of the quadratic equation proposed by ANOVA was evaluated to assess the accuracy of the model. CIP reduction model (Y) based on F test was significant at 95% confidence level (Table 2).

As observed in Table 2, the determination coefficient (R^2) was acceptable, and P-values for model variables were all <0.05, indicating compatibility between the predicted and observed data. Also, the lack of fit F-value was > 0.05, meaning

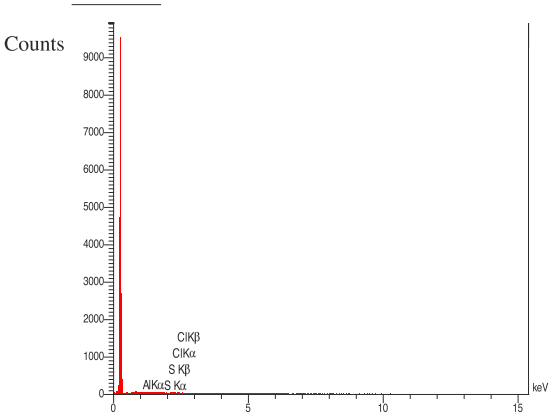

a) Pure MWCNTs

Elt	W%	A%	ZAF
C	99.79	99.91	0.9686
Al	0.11	0.05	0.7200
S	0.07	0.03	0.8774
Cl	0.04	0.01	0.8487
Total	100.00	100.00	

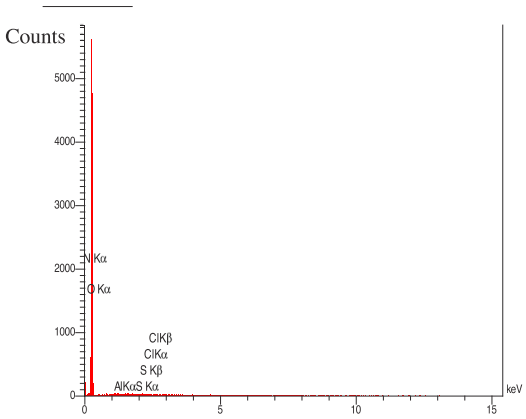

b) Functional MWCNTs

Elt	W%	A%	ZAF
C	78.41	97.19	0.9378
N	6.38	1.19	0.0500
O	15.07	1.57	0.0905
Al	0.05	0.02	0.7122
S	0.03	0.01	0.8755
Cl	0.06	0.02	0.8481
Total	100.00	100.00	

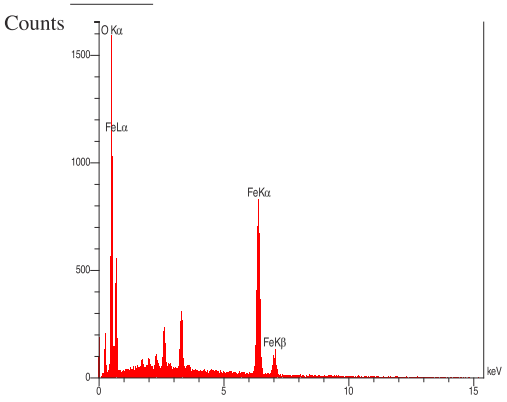

c) Feroxyhyte Nanoparticle

Elt	W%	A%	ZAF
O	50.05	77.77	0.6755
Fe	49.95	22.23	0.8919
Total	100.00	100.00	

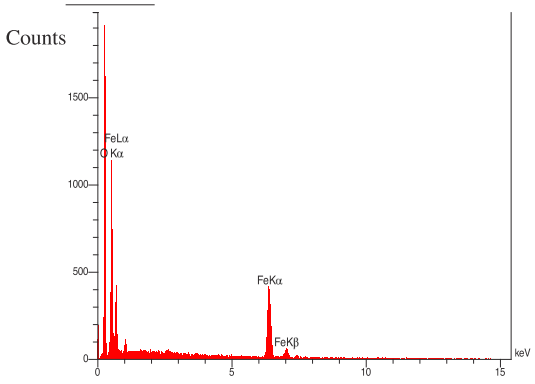

d) Nanocomposite (δ-FeOOH)/MWCNTs

Elt	W%	A%	ZAF
C	51.38	61.54	0.4888
O	30.43	36.35	0.1833
Fe	18.19	2.11	0.7946
Total	100.00	100.00	

Fig. 4. EDX characterizations of samples (a) Pure MWCNTs, (b) Functional MWCNTs (c) Feroxyhyte Nanoparticles, and (d) (δ-FeOOH)/MWCNTs nanocomposite.

that the proposed quadratic model was statistically reasonable. Since the coefficient of variance (CV) (5.30%) was < 10%, the model is acceptable. Furthermore, Adequate Precision (AP), defined as a measure of predicted response domain associated with its related error (or a signal-to-noise ratio), should be four or more (Amiri and Sabour, 2014; Salari et al., 2018a,b, 2019). Since, in this model, AP value (28.20) was more than 4, model performance is satisfactory. Fig. S5 depicts the predicted and normal plots for CIP removal, which match well with the experimental results, confirming the accuracy

Table 1
Design matrix of central composite design (CCD) and CIP degradation results using (δ-FeOOH)/MWCNTs in a Fenton-like process.

Run number	A: CIP Conc., mg/L	B: Nanocomposite dose, mg	C: H_2O_2 Conc, mM	D: pH	E: Time, min	Response: CIP removal (%)	
						Actual value	Predicted value
1	33.0	12.5	10.0	6.5	90.0	72.3	71.0
2	79.0	27.5	20.0	3.5	150.0	60.0	58.5
3	79.0	12.5	10.0	6.5	150.0	59.5	59.3
4	79.0	12.5	20.0	6.5	150.0	62.8	61.7
5	79.0	12.5	20.0	6.5	90.0	71.3	68.5
6	33.0	27.5	10.0	3.5	90.0	70.5	67.8
7	33.0	27.5	10.0	6.5	150.0	67.6	66.2
8	79.0	27.5	20.0	3.5	90.0	62.7	65.3
9	33.0	27.5	20.0	3.5	150.0	65.0	63.4
10	56.0	20.0	5.0	5.0	120.0	64.0	63.9
11	56.0	20.0	15.0	5.0	120.0	58.0	60.5
12	33.0	12.5	20.0	3.5	90.0	69.1	68.2
13	79.0	12.5	10.0	3.5	150.0	54.0	54.1
14	33.0	12.5	10.0	3.5	150.0	58.2	59.0
15	33.0	27.5	10.0	6.5	90.0	67.7	73.0
16	79.0	27.5	10.0	3.5	90.0	63.0	62.9
17	79.0	27.5	10.0	6.5	150.0	58.0	61.3
18	56.0	5.0	15.0	5.0	120.0	54.0	58.6
19	56.0	20.0	15.0	2.0	120.0	38.0	38.6
20	33.0	12.5	20.0	6.5	150.0	68.0	66.5
21	79.0	27.5	20.0	6.5	150.0	66.6	63.7
22	56.0	20.0	25.0	5.0	120.0	62.0	68.7
23	79.0	27.5	20.0	6.5	90.0	75.1	70.5
24	33.0	27.5	10.0	3.5	150.0	62.0	61.0
25	33.0	27.5	20.0	6.5	90.0	79.4	75.3
26	56.0	20.0	15.0	8.0	120.0	43.0	49.0
27	56.0	20.0	15.0	5.0	180.0	62.0	63.0
28	79.0	12.5	10.0	3.5	90.0	62.4	60.9
29	79.0	27.5	10.0	3.5	150.0	57.7	56.1
30	33.0	12.5	20.0	6.5	90.0	75.6	73.3
31	56.0	20.0	15.0	5.0	60.0	71.0	76.6
32	79.0	12.5	10.0	6.5	90.0	68.0	66.1
33	33.0	27.5	20.0	6.5	150.0	68.0	68.5
34	33.0	12.5	10.0	3.5	90.0	66.7	65.8
35	102.0	20.0	15.0	5.0	120.0	68.0	74.2
36	79.0	12.5	20.0	3.5	150.0	57.1	56.5
37	33.0	12.5	20.0	3.5	150.0	61.4	61.4
38	79.0	12.5	20.0	3.5	90.0	65.7	63.3
39	56.0	20.0	15.0	5.0	120.0	68.0	60.5
40	33.0	27.5	20.0	3.5	90.0	66.7	70.2
41	33.0	12.5	10.0	6.5	150.0	63.8	64.2
42	56.0	35.0	15.0	5.0	120.0	61.0	62.5
43	10.0	20.0	15.0	5.0	120.0	83.5	83.9
44	56.0	20.0	15.0	5.0	120.0	61.7	60.5
45	79.0	27.5	10.0	6.5	90.0	71.8	68.1

of the model. However, a perturbation plot is required to examine the response performance (CIP removal %) within the selected range of input parameters and the effect of each parameter on the response (Fig. 5).

3.2.1. Effect of initial CIP concentration

In Fig. 5, parameter A (CIP concentration) has a negative effect on the response performance. It was concluded that an increase in CIP and H_2O_2 concentrations lead to a slight reduction in CIP removal. Table 1 (run #43) shows that the heterogeneous Fenton-like process has the highest removal efficiency (83.5%) for the initial CIP concentration of 10.0 mg/L. It can be argued that higher pollutant concentrations entail higher nanocomposite amounts with a longer required time for treatment.

3.2.2. Effect of nanocomposite dose

In this study, an increase in the nanocomposite dose from 5 to 20 mg, leads to an increase in the effectiveness of CIP removal from 54 to 83.5%, and a further increase in nanocomposite dose up to 35 mg does not significantly change the efficiency. Therefore, 20 mg was selected as the optimal value. As shown in Fig. 5, B (catalyst dosage, mg) has a positive effect on the response since at higher nanocomposite doses, Fe is more available, which increases the decomposition of H_2O_2 and reacts with iron ions. These reactions eventually increase the production of OH^0 radicals in the solution and, consequently, better decomposition of the contaminants (Hu et al., 2011; Xu et al., 2016). Therefore, the optimal amount

Table 2
The ANOVA results for the adequacy of the quadratic model.

Source	Sum of squares	Degree of freedom	Mean square	F value	P-value Prob > F	
Model	2484.25	9	276.03	23.80	< 0.0001	**significant**
A-Initial CIP (mg/L)	236.68	1	236.68	20.41	< 0.0001	
B-Nanocomposite (mg)	39.80	1	39.80	3.43	0.0724	
C-H_2O_2 Concentration	55.93	1	55.93	4.82	0.0348	
D-Initial pH	266.77	1	266.77	23.00	< 0.0001	
E-Time	464.44	1	464.44	40.05	< 0.0001	
A^2	570.57	1	570.57	49.20	< 0.0001	
C^2	55.15	1	55.15	4.76	0.0360	
D^2	467.46	1	467.46	40.31	< 0.0001	
E^2	142.68	1	142.68	12.30	0.0013	
Residual	405.91	35	11.60			
Lack of Fit	354.79	33	10.75	0.42	0.8915	**not significant**
Pure Error	51.13	2	25.56			

Std Dev = 3.41, CV% = 5.30, PRESS = 983.1, R^2 = 0.85, Adj. R^2 = 0.82, Adequate precisions = 28.2.

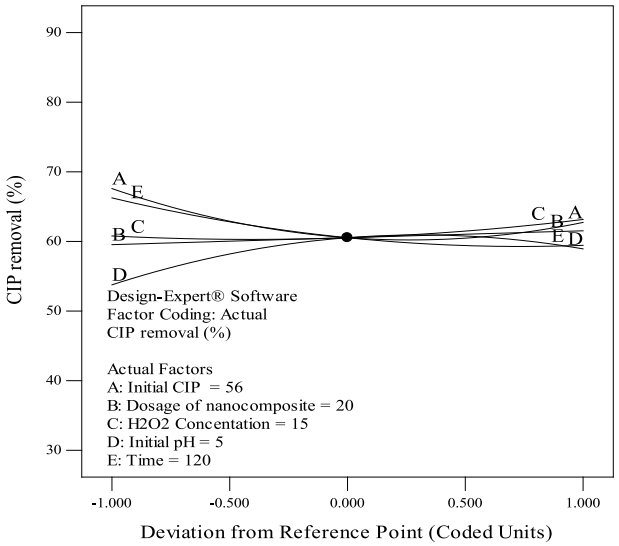

Fig. 5. Perturbation plot of variables for CIP removal in the Fenton-like process.

of nanocomposite is sufficient to increase CIP degradation. Also, significant removal efficiency results in the reduction of process cost at the optimal value (Li et al., 2014).

3.2.3. *Effect of initial pH on CIP degradation*

The ionized CIP molecule contains two proton binding sites, including the carboxylic acid ($pKa_1 = 5.9 \pm 0.15$) and amine ($pKa_2 = 8.89 \pm 0.11$) groups (Fig. S6). Thus, its dominant forms at pH <5.9 ± 0.15 are cationic (CIP^+) due to the protonation of the secondary amine in piperazine, and the leading forms at pH > 8.89 ± 0.11 are anionic (CIP^-) due to proton loss from the carboxylic group. Additionally, at pH = 6.1–8.7, the dominant form is zwitterionic or neutral ($CIP^{\pm}/CIP^0$) (Peng et al., 2015). Fig. S6 shows various ionic forms of CIP.

Based on Fig. S4, PZC of MWCNTs is ∼3.92 since surface charge at pH values < pHpzc is positive (Peng et al., 2015). At pH < 5.9 ± 0.15, CIP and adsorbent surface have opposite charges, and thus due to similar charge repellence, adsorption is expected to be diminished. At pH values in the 5–6 range, due to the opposite charge of CIP molecules and nanotubes, inductive electrostatic absorption results in absorption rate enhancement.

pH_{pzc} of the nanocomposite was ∼4.36. At pH < 4.36, due to a positive charge, the electrostatic repulsion force will reduce the adsorption rate of CIP. At pH values between 6–8, electrostatic induction force increases adsorption due to the opposite surface charge of MWCNT and CIP molecule. Therefore, electrostatic interaction between CIP and the adsorbent is considered one of the major factors influencing the adsorption. Also, at pH > 8, electrostatic repulsion between negative charges reduces the adsorption rate of CIP (Chen and Huang, 2010). Overall, the highest removal efficiency was obtained at pH = 5.

3.2.4. Effect of reaction time

Reaction time is considered as one of the most important variables for the design and management of the treatment process. Due to a large number of adsorption sites in the early stages of the reaction, the adsorption rate is high (Li et al., 2014). The most effective CIP antibiotic removal (83.5%) was achieved over 120 min, after which the adsorption is gradually decreased (Table 1, run#43). Based on the CCD model prediction, optimal conditions for CIP removal were determined in an initial CIP concentration of 10.0 mg/L, a catalyst dose of 23.5 mg, H_2O_2 concentration of 20.6 mM, initial pH of 5.3, and 131.6 min for reaction time. Under these conditions, the maximum predicted value for CIP removal was 84.5%, while the corresponding experimental value was 86.9%, which is very close to the predicted value with a 2.7% absolute deviation (Table S2).

Before treatment, the BOD_5 value of the solution was very low and close to zero, which confirms the difficulty of wastewater treatment by traditional techniques such as biological treatment. Upon treatment, the biodegradability index was calculated to be 0.35, which shows the suitable function of the proposed process and reducing the toxicity by increasing the biocompatibility of CIP solution, enabling the process to be combined with a biological process. Overlapped HPLC chromatograms at 277 nm show CIP degradation efficiency using Fenton-like removal under optimal conditions (Fig. S7). According to Fig. S7, the highest peak in CIP adsorption is reduced with reaction time, which indicates the decomposition of CIP and transformation into other compounds.

3.2.5. Evaluation of antibacterial activity

As shown in Fig. S8, E. coli grew continuously over time, and 180 min after bacterial growth, it appeared in most parts of the plate. As a result, there was a significant inhibitor in the plate, and antibiotics were removed. In other words, the effect of antibacterial control, especially on the plates (e), was very low in both growth environments (BA and EMBA). Therefore, antibacterial activity was very low after treatment.

4. Summary and conclusion

This study investigates an optimized heterogeneous Fenton-like process for CIP removal , in which (δ-FeOOH)/MWCNTs nanocomposite was synthesized and characterized using a single-step co-precipitation technique without toxic, organic, or expensive precursors. The effect of influential variables was also assessed throughout the process optimization. A notable point in this study was using cheap and affordable raw materials and the relatively simple nanocomposite that may be considered a suitable high-performance catalyst for the degradation of organic compounds. Also, RSM based on central composite design (CCD) was successfully applied, and experiments were designed based on five input variables (i.e., initial CIP concentration, catalyst dose, H_2O_2 concentration, initial pH, and reaction time). The mechanism of catalyst performance was the synergistic effect of both advanced oxidation processes (Fenton-like) and adsorption. The proposed methodology not only increases the efficiency of advanced oxidation but also reduces the cost by decreasing the required concentration of hydrogen peroxide. CCD method predicted CIP removal effectively (R^2 = 0.85). Moreover, the optimal CIP removal efficiency (86.9%) was achieved at a 131.6 min reaction time, CIP concentration of 10.0 mg/l, catalyst dose of 23.5 mg, H_2O_2 concentration of 20.6 mM, and initial pH of 5.3. In order to validate the optimization results, two confirmatory experiments were conducted at the optimal operating conditions (Table S2). To verify model prediction, biodegradability index (BOD_5/COD) was determined (0.35), which showed that the effluent could be treated by a biological process. Experimental results showed that a uniform distribution of iron oxide nanostructures on MWCNTs was achieved. Therefore, according to the inhibitory hale experiment by Escherichia coli (E. coli), antibacterial activity after treatment was very low in both growth environments (BA and EMBA). Based on the results, (δ-FeOOH)/MWCNTs showed an efficient catalytic activity for CIP removal, which may be attributed to the simultaneous effect of advanced oxidation and adsorption. Low cost and simple preparation procedure encourage future investigations on the design of new types of composites like (δ-FeOOH)/MWCNT.

CRediT authorship contribution statement

Marjan Salari: Investigation, Methodology, Formal analysis, Designed and performed experiments, Data analyses, Writing - review & editing. **Gholam Reza Rakhshandehroo:** Supervision, Conceptualization, Data analyses, Investigation, Writing - review & editing. **Mohammad Reza Nikoo:** Supervision, Conceptualization, Data analyses, Investigation, Writing - review & editing. **Mohammad Mahdi Zerafat:** Supervision, Conceptualization, Writing - review & editing. **Mehrdad Ghorbani Mooselu:** Conceptualization, Writing - review & editing.

Declaration of competing interest

The authors declare that they have no known competing financial interests or personal relationships that could have appeared to influence the work reported in this paper.

Appendix A. Supplementary data

Supplementary material related to this article can be found online at https://doi.org/10.1016/j.eti.2021.101625.

References

Aboutalebi, S.H., Chidembo, A.T., Salari, M., Konstantinov, K., Wexler, D., Liu, H.K., Dou, S.X., 2011. Comparison of GO, GO/MWCNTs composite and MWCNTs as potential electrode materials for supercapacitors. Energy Environ. Sci. 4 (5), 1855–1865, https://doi.org/10.1039/C1EE01039E.

Alexander, L., Klug, H.P., 1950. Determination of crystallite size with the X-ray spectrometer. J. Appl. Phys. 21 (2), 137–142, https://doi.org/10.1063/1.1699612.

Amiri, A., Sabour, M.R., 2014. Multi-Response Optimization of Fenton Oxidation for Applicability Assessment in LandFill Leachate Treatment. Waste Manag. 34 (12), 2528–2536, 10.1016/j.wasman.2014.08.010.

Andrews, R., Jacques, D., Rao, A.M., Rantell, T., Derbyshire, F., Chen, Y., Chen, J., Haddon, R.C., 1999. Nanotube composite carbon fibers. Appl. Phys. Lett. 75 (9), 1329–1331, https://doi.org/10.1063/1.124683.

Asghar, A., AbdulRaman, A.A., Wan Daud, W.A., 2014. A comparison of central composite design and taguchi method for optimizing fenton oxidation. Hindawi publishing corporation. Sci. World J. 14, http://dx.doi.org/10.1155/2014/869120.

Azami, M., Bahram, M., Nouri, S., Naseri, A., 2012. Central composite design for the optimization of removal of the azo dye, methyl orange, from waste water using fenton reaction. J. Serb. Chem. Soc. 77 (2), 235–246, https://doi.org/10.5277/ppmp170230.

Carlson, L., Schwertmann, U., 1980. Natural occurrence of feroxyhyte (8'-FeOOH). Clays Clay Miner. 28 (4), 272–280, https://doi.org/10.1346/CCMN.1980.0280405.

Chen, X.H., Chen, C.S., Xiao, H.N., Cheng, F.Q., Zhang, G., YI, G.J., 2005. Corrosion behavior of carbon nanotubes-Ni composite coating. Surf. Coat. Tech. 191, 351–356, https://doi.org/10.1016/j.surfcoat.2004.04.055.

Chen, W.R., Huang, C.H., 2010. Adsorption and transformation of tetracycline antibiotics with aluminum oxide. Chemosphere 79 (8), 779–785. http://dx.doi.org/10.1016/j.chemosphere.2010.03.020.

Chen, C.S., Liu, X.H., Lin, L.W., Liu, Q.C., Qing, X.I.A., Ning, Z.W., 2009. Preparation and magnetic property of multi-walled carbon nanotube/α-Fe_2O_3 composites. Trans. Nonferrous Met. Soc. China 19 (6), 1567–1571, https://doi.org/10.1016/S1003-6326(09)60071-6.

Chen, X.H., Zhang, G., Chen, C.S., Zhou, L.P., Li, S., Li, X., 2003. Carbon nanotube composite deposits with high hardness and high wear resistance. Eng. Mater. 5 (7), 514–518, https://doi.org/10.1002/adem.200300348.

Chen, H., Zhang, Z.L., Yang, Z.L., 2015. Heterogeneous fenton-like catalytic degradation of 2, 4-dichlorophenoxyacetic acid in water with fes. Chem. Eng. J. 273, 481–489, http://dx.doi.org/10.1016/j.cej.2015.03.079.

Cui, Z.M., Chen, Z., Cao, C.Y., Jiang, L., Song, W.G., 2013. A yolk–shell structured Fe_2O_3@ mesoporous Sio2 nanoreactor for enhanced activity as a Fenton catalyst in total oxidation of dyes. Chem. Commun. 49 (23), 2332–2334, https://doi.org/10.1039/C3CC38649J.

De Lima Perini, J.A., Silva, B.F., Nogueira, R.F.P., 2014. Zero-valent iron mediated degradation of ciprofloxacin–assessment of adsorption, operational parameters and degradation products. Chemosphere 117, 345–352. http://dx.doi.org/10.1016/j.chemosphere.2014.07.071.

DeBel, E., Dewulf, J., Van Lagenhove, H., Janssen, C., 2009. Influence of pH on the sonolysis of Ciprofloxacin: biodegradability, ecotoxicity and antibiotic activity of its degradation products. Chemosphere 77, 291–295. http://dx.doi.org/10.1016/j.chemosphere.2009.07.033.

Dhinakaran, R., Elansezhian, R., Arumugam Lalitha1, A., 2013. Effect of nanoadditives with surfactant on the surface characteristics of electroless nickel coating on magnesium-based composites reinforced with MWCNT. Adv. Tribol. 10, 315965, https://doi.org/10.1155/2013/315965.

Fayazi, M., Ghanei-Motlagh, M., Taher, M., 2015. The adsorption of basic dye (Alizarin red S) from aqueous solution onto activated carbon/γ-Fe_2O_3 nanocomposite: Kinetic and equilibrium studies. Mater. Sci. Semicond. Process 40, 35–43. http://dx.doi.org/10.1016/j.mssp.2015.06.044.

Garrido-Ramírez, E.G., Theng, B.K.G., Mora, M.L., 2010. Clays and oxide minerals as catalysts and nanocatalysts in Fenton-like reactions (review). Appl. Clay Sci. 47 (3–4), 182–192, https://doi.org/10.1016/j.clay.2009.11.044.

Giri, A.S., Golder, A.K., 2015. Decomposition of drug mixture in Fenton and photo-Fenton processes: comparison to singly treatment, evolution of inorganic ions and toxicity assay. Chemosphere 127, 254–261. http://dx.doi.org/10.1016/j.chemosphere.2015.02.010.

Golovko, O., Kumar, V., Fedorova, G., Randak, T., Grabic, R., 2014. Seasonal changes in antibiotics, antidepressants/psychiatric drugs, antihistamines and lipid regulators in a wastewater treatment plant. Chemosphere 111, 418–426. http://dx.doi.org/10.1016/j.chemosphere.2014.03.132.

Gul, H., Lu, W., Xu, P., Xing, J., Chen, J., 2010. Magnetic carbon nanotube labelling for haematopoietic stem/progenitor cell tracking. J. Chen Nanotechnology 21 (15), 155101. http://dx.doi.org/10.1088/0957-4484/21/15/155101.

Gupta, A., Garg, A., 2018. Degradation of Ciprofloxacin using Fenton's oxidation: Effect of operating parameters, identification of oxidized by-products and toxicity assessment. Chemosphere 193, 1181–1188, https://doi.org/10.1016/j.chemosphere.2017.11.046.

Haddad, T., Kümmerer, K., 2014. Characterization of photo-transformation products of the antibiotic drug Ciprofloxacin with liquid chromatography–tandem mass spectrometry in combination with accurate mass determination using an LTQ-Orbitrap. Chemosphere 115, 40–46. http://dx.doi.org/10.1016/j.chemosphere.2014.02.013.

Hernando, M.D., Mezcu, M., Fernandez-Alb, A.R., Bercelo, D., 2006. Environmental risk assessment of pharmaceutical residues in wastewater effluents, surface waters and sediments. Talanta 69, 334–342. http://dx.doi.org/10.1016/j.talanta.2005.09.037.

Hu, X., Liu, B., Deng, Y., Chen, H., Luo, S., Sun, C., Yang, P., Yang, S., 2011. Adsorption and heterogeneous Fenton degradation of 17α-methyltestosterone on nano Fe_3O_4/MWCNTs in aqueous solution. Appl. Catal. B 107 (3–4), 274–283, https://doi.org/10.1016/j.apcatb.2011.07.025.

Iurascu, B., Siminiceanu, I., Vione, D., Vicente, M.A., Gil, A., 2009. Phenol degradation in water through a heterogeneous photo-Fenton process catalyzed by Fe-treated laponite. Water Res. 43 (5), 1313–1322, 10.1016/j.watres.2008.12.032.

Kakavandi, B., Takdastan, A., Jaafarzadeh, N., Azizi, M., Mirzaei, A., Azari, A., 2016. Application of Fe_3O_4@C catalyzing heterogeneous UV-Fenton system for tetracycline removal with a focus on optimization by a response surface method. J. Photochem. Photobiol. A Chem. 314, 178–188. http://dx.doi.org/10.1016/j.jphotochem. 08.008.

Kasiri, M.B., Aleboyeh, H., Aleboyeh, A., 2008. Degradation of acid blue 74 using Fe-ZSM5 zeolite as a heterogeneous photo-Fenton catalyst. Appl. Catal. B 84 (1–2), 9–15, https://doi.org/10.1016/j.apcatb.2008.02.024.

Kaur, S., Bhalla, V., Kumar, M., 2015. Facile decoration of multiwalled carbon nanotubes with hetero-oligophenylene stabilized-gold nanoparticles: Visible light photocatalytic degradation of rhodamine B dye. ACS Appl. Mater. Interfaces 7 (30), 16617–16624. http://dx.doi.org/10.1021/acsami.5b04179.

Khataee, A.R., Safarpour, M., Zarei, M., Aber, S., 2012. Combined heterogeneous and homogeneous photodegradation of a dye using immobilized TiO_2 nanophotocatalyst and modified graphite electrode with carbon nanotubes. J. Mol. Catal. A Chem. 363, 58–68, https://doi.org/10.1016/j.molcata.2012.05.016.

Khodadadi, M., Ehrampoush, M.H., Ghaneian, M.T., Allahresani, A., Mahvi, A.H., 2017. Synthesis and characterizations of $FeNi_3$@SiO_2@TiO_2 nanocomposite and its application in photo- catalytic degradation of tetracycline in simulated wastewater. J. Mol. Liq. 225, 224–232.

Kümmerer, K., 2004. Resistance in the environment. J. Antimicrob. Chemother. 54, 311–320. http://dx.doi.org/10.1093/jac/dkh325.

Kümmerer, K., 2009. Antibiotics in the aquatic environment - A review - Part I. Chemosphere 75, 417–434, 10.1016/j.chemosphere.2008.11.086.

Kuzumaki, T., Miyazawa, K., Ichinose, H., Ito, K., 1998. Processing of carbon nanotube reinforced aluminum composites. J. Mater. Res. 13 (9), 2445–2449. http://dx.doi.org/10.1016/j.chemosphere.2008.11.086.

Lak, M.G., Sabour, M.R., Amiri, A., Rabbani, O., 2012. Application of quadratic regression model for Fenton treatment of municipal landfill leachate. Waste Manag. 32 (10), 1895–1902. http://dx.doi.org/10.1016/j.wasman.2012.05.020.

Levy, S., 1998. The challenge of antibiotic resistance. Sci. Am. 278, 46–53. http://dx.doi.org/10.1038/scientificamerican0398-46.
Li, H., Zhang, D., Han, X., Xing, B., 2014. Adsorption of antibiotic Ciprofloxacin on carbon nanotubes: Ph dependence and thermodynamics. Chemosphere 95, 150–155. http://dx.doi.org/10.1016/j.chemosphere.2013.08.053.
Lima, M.J., Silva, C.G., Silva, A.M., Lopes, J.C., Dias, M.M., Faria, J.L., 2017. Homogeneous and heterogeneous photo-Fenton degradation of antibiotics using an innovative static mixer photoreactor. Chem. Eng. J. 310, 342–351, 10.1016/j.cej.2016.04.032.
Maa, J., Yang, M., Yu, F., Chen, J., 2015. Easy solid-phase synthesis of pH-insensitive heterogeneous CNTs/FeS Fenton-like catalyst for the removal of antibiotics from aqueous solution. J. Colloid Interface Sci. 444, 24–32. http://dx.doi.org/10.1016/j.jcis.2014.12.027.
Nie, Y., Zhang, L., Li, Y., 2015. Enhanced Fenton-like degradation of refractory organic compounds by surface complex formation of $LaFeO_3$ and H_2O_2. J. Hazard Mater. 294, 195–200. http://dx.doi.org/10.1016/j.jhazmat.2015.03.065.
Peng, X., Lam, F.L.Y., Wang, Y., Liu, Z., 2015. Adsorption behavior and mechanisms of Ciprofloxacin from aqueous solution by ordered mesoporous carbon and bamboo-based carbon. J. Colloid Interface Sci. 460, 349–360, http://dx.doi.org/10.1016/j.jcis.2015.08.050.
Rakhshandehroo, G.R., Salari, M., Nikoo, M.R., 2018. Optimization of degradation of ciprofloxacin antibiotic and assessment of degradation products using full factorial experimental design by Fenton homogenous process. Glob. Nest J. 20 (2), 324–332, https://doi.org/10.30955/gnj.002537.
Salari, M., Rakhshandehroo, G.R., Nikoo, M.R., 2018a. Multi-objective optimization of ciprofloxacin antibiotic removal from an aqueous phase with grey taguchi method. J. Water Health 16 (4), 530–541. http://dx.doi.org/10.2166/wh.2018.247.
Salari, M., Rakhshandehroo, G.R., Nikoo, M.R., 2018b. Degradation of Ciprofloxacin antibiotic by homogeneous Fenton oxidation: Hybrid AHP-PROMETHEE method, optimization, biodegradability improvement and identification of oxidized by-products. Chemosphere 206, 157–167. http://dx.doi.org/10.1016/j.chemosphere.2018.04.086.
Salari, M., Rakhshandehroo, G.R., Nikoo, M.R., 2019. Developing multi-criteria decision analysis and taguchi method to optimize ciprofloxacin removal from aqueous phase. Environ. Eng. Manag. J. 18 (7), 1543–1552, http://www.eemj.icpm.tuiasi.ro/; http://www.eemj.eu.
Sestu, M., Carta, D., Casula, M.F., Corrias, A., Navarra, G., 2015. Novel interpretation of the mean structure of feroxyhyte. J. Solid State Chem. 225, 256–260, http://epubs.surrey.ac.uk/id/eprint/842068.
Shahidi, S., Mazaheri, F., Moazzenchi, B., Hoseini, H., 2018. Studying the magnetic, antibacterial, and catalytic activity properties of DBD/iron oxide nanoparticle-treated cotton fabric. J. Nat. Fibers 1–9, https://doi.org/10.1080/15440478.2017.1361372.
Shukla, P., Wang, S., Sun, H., Ang, H.M., Tadé, M., 2010. Adsorption and heterogeneous advanced oxidation of phenolic contaminants using Fe loaded mesoporous SBA-15 and H_2O_2. Chem. Eng. J. 164 (1), 255–260, https://doi.org/10.1016/j.cej.2010.08.061111117.
Wan, D., Li, W., Wang, G., Chen, K., Lu, L., Hu, Q., 2015. Adsorption and heterogeneous degradation of rhodamine B on the surface of magnetic bentonite material. Appl. Surf. Sci 349, 988–996, https://doi.org/10.1016/j.apsusc.2015.05.004.
Watkinson, A.J., Murby, S.D., Costanzo, E.J., 2007. Removal of antibiotics in conventional and advanced wastewater treatment: implications for environmental discharge and wastewater recycling. Water Res. 41, 4164–4176. http://dx.doi.org/10.1016/j.watres.2007.04.005.
Xu, H.Y., Shi, T.N., Zhao, H., Jin, L.G., Wang, F.C., Wang, C.Y., Qi, S.Y., 2016. Heterogeneous Fenton-like discoloration of methyl orange using Fe_3O_4/MWCNTs as catalyst: process optimization by response surface methodology. Front Mater. Sci. 10 (1), 45–55. http://dx.doi.org/10.1007/s11706-018-0408-1.
Xu, C.L., Wei, B.Q., Ma, R.Z., Liang, J., Ma, X.K., Wu, D.H., 1999. Fabrication of aluminum-carbon nanotube composites and their electrical properties. Carbon 37 (5), 855–858, https://doi.org/10.1016/S0008-6223(98)00285-1.
Yao, Y., Qin, J., Cai, Y., Wei, F., Lu, F., Wang, S., 2014. Facile synthesis of magnetic $ZnFe_2O_4$–reduced graphene oxide hybrid and its photo-Fenton-like behavior under visible iradiation. Environ. Sci. Pollut Res. Int. 21 (12), 7296–7306, https://doi.org/10.1007/s11356-014-2645-x.
Ye, J.S., Liu, J., Ou, H., Wang, L.L., 2016. Degradation of Ciprofloxacin by 280 nm ultraviolet-activated persulfate: degradation pathway and intermediate impact on proteome of escherichia coli. Chemosphere 165, 311–319, https://doi.org/10.1016/j.chemosphere.2016.09.031.
Yeh, C.K.J., Hsu, C.Y., Chiu, C.H., Huang, K.L., 2008. Reaction efficiencies and rate constants for the goethite-catalyzed Fenton-like reaction of NAPL-form aromatic hydrocarbons and chloroethylenes. J. Hazard Mater. 151 (2–3), 562–569, 10.1016/j.jhazmat.2007.06.014.
Zhan, G.D., Kuntz, J.D., Wan, J.L., Mukherjee, A.K., 2003. Single-wall carbon nanotubes as attractive toughening agents in aluminabased nanocomposites. Nat. Mater. 2 (1), 38–42. http://dx.doi.org/10.1038/nmat793.
Zhang, L.S., Wong, K.H., Yip, H.Y., Hu, C., Yu, J.C., Chan, C.Y., Wong, P.K., 2010. Effective photocatalytic disinfection of E. coli K-12 using AgBr $^{-}$ Ag^{-} Bi_2 WO6 nanojunction system irradiated by visible light: the role of diffusing hydroxyl radicals. Environ. Sci. Technol. 44 (4), 1392–1398, https://doi.org/10.1021/es903087w.
Zhuang, Y., Yu, F., Ma, J., Chen, J.H., 2015. Adsorption of Ciprofloxacin onto graphene–soy protein biocomposites. New J. Chem. 39, 3333–3336, https://doi.org/10.1039/C5NJ00019J.
Zubir, N.A., Yacou, C., Motuzas, J., Zhang, X., Zhao, X.S., Da Costa, J.C.D., 2015. The sacrificial role of graphene oxide in stabilising a Fenton-like catalyst GO–Fe_3O_4. Chem. Commun. 51 (45), 9291–9293, https://doi.org/10.1039/C5CC02292D.